

A CWENO large time-step scheme for Hamilton–Jacobi equations

E. Carlini, R. Ferretti, S. Preda, and M. Semplice

Abstract

We propose a high order numerical scheme for time-dependent first order Hamilton–Jacobi–Bellman equations. In particular we propose to combine a semi-Lagrangian scheme with a Central Weighted Non-Oscillatory reconstruction. We prove a convergence result in the case of state- and time-independent Hamiltonians.

Numerical simulations are presented in space dimensions one and two, also for more general state- and time-dependent Hamiltonians, demonstrating superior performance in terms of CPU time gain compared with a semi-Lagrangian scheme coupled with Weighted Non-Oscillatory reconstructions.

Keywords: semi-Lagrangian schemes, Hamilton–Jacobi equations, CWENO methods

AMS Subject Classification: Primary, 65N12, 65M10; Secondary, 49L25

1 Introduction

In this paper, we address the numerical approximation of the following hyperbolic Hamilton–Jacobi–Bellman (HJB) equation:

$$\begin{cases} v_t(t, x) + H(t, x, Dv(t, x)) = 0, & \text{for } t, x \in (0, T) \times \mathbb{R}^d, \\ v(0, x) = v_0(x), & \text{for } x \in \mathbb{R}^d, \end{cases} \quad (1.1)$$

where $v : (0, T) \times \mathbb{R}^d \rightarrow \mathbb{R}$, Dv stands for the spatial gradient, and $H : (0, T) \times \mathbb{R}^d \times \mathbb{R}^d \rightarrow \mathbb{R}$.

Numerous schemes have been proposed to approximate (1.1), but only a small number are aimed at high order accuracy. High order finite difference schemes based on ENO (Essentially Non-Oscillatory) reconstruction, defined in [HEOC87], were proposed in [OS91] and extended to unstructured grids in [Abg94]. Second order Godunov-type schemes based on global projection operators are discussed in [LT00]. Weighted ENO (WENO) schemes were introduced in [JS96, LOC94] and combined with finite difference schemes for Hamilton–Jacobi (HJ) equations in [JP00]. A fifth order central scheme based on WENO reconstruction has been developed in [HT03].

Over the past two decades, semi-Lagrangian (SL) schemes have been employed to discretize the HJ equation. In [FF94], a high order semi-discrete SL scheme is proposed to discretize stationary HJB equations, while in [FF02], SL schemes are applied to evolutionary HJB equations. A high order SL scheme for HJB equations is presented in [CFR06] by combining the SL technique with WENO reconstructions.

A different approach to achieve high order accuracy involves filtered schemes. In [BFS16, FPT20a], filtered schemes are combined with monotone finite difference schemes to discretize first order evolutionary HJ equations.

For an overview of numerical methods for first order Hamilton–Jacobi equations, we also refer to the book [FF14].

We will develop our theory for the HJB equation related to a finite horizon optimal control. More precisely, given a compact $A \in \mathbb{R}^m$, let the set $\mathcal{A} = \{\alpha : [0, T] \rightarrow A, \text{ measurable}\}$ denote the admissible controls. Given the running cost $f_C : (0, T) \times \mathbb{R}^d \times A \rightarrow \mathbb{R}$ and the dynamics $f_D : (0, T) \times \mathbb{R}^d \times A \rightarrow \mathbb{R}^d$ for the system

$$\dot{y}(s) = f_D(t - s, y(s), \alpha(s)), \quad s \in (0, t], \quad y(0) = x, \quad (1.2)$$

we consider the following Hamiltonian

$$H(t, x, p) = \max_{a \in A} (-f_D(t, x, a) \cdot p - f_C(t, x, a)). \quad (1.3)$$

Let us assume that

(H1) f_C, f_D are continuous and bounded. Moreover, for every $a \in A$, the functions $f_C(\cdot, \cdot, a)$, $f_D(\cdot, \cdot, a)$ are Lipschitz continuous, with Lipschitz constants independent of $a \in A$.

(H2) v_0 is Lipschitz continuous and bounded.

Under Assumptions **(H1)**–**(H2)**, problem (1.1) admits a unique viscosity solution v , which is Lipschitz continuous and bounded. Moreover, the Dynamic Programming Principle holds (see [BCD97, Chapter 3], i.e., for any $h > 0$

$$v(t, x) = \inf_{\alpha \in \mathcal{A}} \left\{ \int_0^h f_C(t - s, y_{x,t}(s), \alpha(s)) ds + v(y_{x,t}(h), t - h) \right\}, \quad (1.4)$$

where $y_{x,t}$ denotes the solution to (1.2).

A numerical scheme based on the previous description involves a minimization procedure over the set of controls; in turn, each function evaluation requires to approximate the cost integral and to interpolate the solution at the previous time step at the foot $y_{x,t}(h)$ of the characteristics. In this respect, WENO reconstructions, especially in higher space dimensions, are not efficient, due to fact that the linear weights of WENO depend on the reconstruction point.

A novel paradigm for non-oscillatory reconstruction operators has been introduced in [LPR00], where the authors suggested to blend, in a WENO-like fashion, polynomials of different degrees, allowing to overcome some difficulties of non-existence, non-positivity and dependence on the reconstruction point of the WENO linear weights. The idea has been further developed into the so-called CWENO reconstruction and exploited in more spatial dimensions, also in the case of adaptive mesh refinement and non-uniform grids [BGFB20, ZQ16, BBMZ19, ZCZ08, DBSR17]. The technique has also been exploited in finite difference schemes for Hamilton-Jacobi equations on Cartesian meshes via dimensional splitting [ZQ17, ZSQ19] and on general meshes [ZQ20]. General results for establishing the convergence order of a CWENO reconstruction have been presented in [CPSV18, CSV19, SV20].

One of the main advantages of CWENO over the traditional WENO is that the central approach provides a reconstruction polynomial that is defined everywhere in the reconstruction cell and that can be evaluated later, with no essential extra cost, at many different reconstruction points. This is guaranteed by the independence of the linear weights from the reconstruction point. Furthermore, as shown in [SCR16, DBSR17, CS19, CPSV18], the CWENO approach allows to avoid the dimensional splitting procedure and this is advantageous also on Cartesian meshes when the number of reconstruction points per cell is high.

In this paper we want to exploit the positive features of CWENO to obtain a high order SL scheme that is more efficient than the one of [CFR06], which are based on WENO. The rest of the paper is organized as follows. In §2 the general principles of the SL scheme are recalled, whereas in §3 a CWENO interpolation from point values is constructed in one and two space dimensions. §4 proves a convergence result in the framework of [Fer02], and finally §5 provides an extensive number of numerical examples to validate the scheme.

2 Numerical scheme

To obtain an approximate version of (1.1), we need first to discretize the control problem in time. Let $\Delta t > 0$ be a time step, $t_n = n\Delta t$ a uniform time grid with $n = 0, \dots, N_T$, where $N_T = \lceil \frac{T}{\Delta t} \rceil$, and consider the Dynamic Programming Principle on a single time step $[t_n, t_{n+1}]$, by choosing in (1.4) $h = \Delta t$ and $t = t_{n+1}$.

When using a ν -stages scheme for (1.2), we discretize an admissible control $\alpha \in \mathcal{A}$ via a sequence $\underline{a} = (a_1, a_2, \dots, a_\nu) \in A^\nu$. Then the foot of the characteristic corresponding to the control \underline{a} is

$$y^n(x, \underline{a}) \simeq y_{x, t_{n+1}}(\Delta t)$$

for any $n = 0, \dots, N_T - 1$, $x \in \mathbb{R}^d$ and $\underline{a} \in A^\nu$.

Moreover, a suitable quadrature formula based on ν quadrature nodes is introduced to discretize the integral term related to the running cost,

$$C^n(x, \underline{a}) \simeq \int_0^{\Delta t} f_C(t_{n+1} - s, y_{x, t_{n+1}}(s), \alpha(s)) ds,$$

for any $n = 0, \dots, N_T - 1$, $x \in \mathbb{R}^d$ and $\underline{a} \in A^\nu$.

Let us now introduce the space grid with space step Δx so that $x_i = i\Delta x$ with $i \in \mathbb{Z}^d$ and denote $y_i^n(\underline{a}) = y^n(x_i, \underline{a})$ and $C_i^n(\underline{a}) = C^n(x_i, \underline{a})$. We approximate the solution $v(x, t)$ of (1.1) by a discrete function $u_i^n \simeq v(x_i, t_n)$ defined on the space-time grid, computed by the following iterative scheme, for $n = 0, \dots, N_T - 1$

$$\begin{cases} u_i^{n+1} = \min_{\underline{a} \in A^\nu} \{R[u^n](y_i^n(\underline{a})) + C_i^n(\underline{a})\} & i \in \mathbb{Z}^d, \\ u_i^0 = v_0(x_i), & i \in \mathbb{Z}^d, \end{cases} \quad (2.1)$$

where $R[u^n](x)$ denotes the spatial reconstruction at $x \in \mathbb{R}^d$ of the numerical solution $u^n = (u_i^n)_{i \in \mathbb{Z}^d}$.

For a given $\underline{a} \in A^\nu$, $y_i^n(\underline{a})$ is computed via a ν -stage Runge–Kutta (RK) methods as follows:

$$\begin{aligned} y_i^n(\underline{a}) &= x_i + \Delta t \sum_{k=1}^{\nu} b_k K_k(\underline{a}), \\ K_k(\underline{a}) &= f_D(t_n + (1 - c_k)\Delta t, X_k(\underline{a}), a_k), \\ X_k(\underline{a}) &= x_i + \Delta t \sum_{j=1}^{k-1} A_{kj} K_j(\underline{a}), \end{aligned} \quad (2.2)$$

where b_k, c_k, A_{kj} are the coefficients of the Butcher tableau defining the RK method used to solve (1.2). For our purposes, we resort to the Forward Euler method for first order schemes, to

Heun's method

$$\begin{array}{c|cc} 0 & & \\ 1 & 1 & \\ \hline & 1/2 & 1/2 \end{array} \quad (2.3)$$

to get second order accuracy, and to RK method with tableau

$$\begin{array}{c|ccc} 0 & & & \\ 1/2 & 1/2 & & \\ 1 & -1 & 2 & \\ \hline & 1/6 & 2/3 & 1/6 \end{array} \quad (2.4)$$

to get third order accuracy.

In order to compute $C_i^n(\underline{a})$, we employ a suitable quadrature rule and replace the function evaluations at the nodes with the numerical solution of (1.2):

$$\begin{aligned} & \int_0^{\Delta t} f_C(t_{n+1} - s, y_{x_i, t_{n+1}}(s), \alpha(s)) ds \\ = & \Delta t \sum_k w_k f_C(t_{n+1} - \xi_k \Delta t, y_{x_i, t_{n+1}}(\xi_k \Delta t), \alpha(\xi_k \Delta t)) + \mathcal{O}(\Delta t^{Q+1}) \\ = & \Delta t \sum_k w_k f_C(t_{n+1} - \xi_k \Delta t, \tilde{y}_{x_i, t_{n+1}}(\xi_k \Delta t), \alpha(\xi_k \Delta t)) + \mathcal{O}(\Delta t^{Q+1} + \Delta t^{R+1}) \end{aligned} \quad (2.5)$$

where ξ_k, w_k are the nodes and the weights of the quadrature rule and $\tilde{y}_{x_i, t_{n+1}}(\xi_k \Delta t)$ is a suitable approximation of the numerical solution of $y_{x_i, t_{n+1}}(s)$ for $s \in [0, \Delta t]$; Q is the accuracy of the quadrature rule and R describes the extra error introduced by the approximation of $y_{x_i, t_{n+1}}(\xi_k \Delta t)$ with $\tilde{y}_{x_i, t_{n+1}}(\xi_k \Delta t)$ within the quadrature rule. It is tempting to choose a quadrature rule whose nodes coincide with the abscissae $\{c_k\}$ of the RK scheme and replace, in the last approximation of (2.5), $\tilde{y}_{x_i, t_{n+1}}(\xi_k \Delta t)$ with the stage values of the RK scheme X_k and $\alpha(\xi_k \Delta t)$ with a_k , for $k = 1, \dots, \nu$.

For the Heun method, the numerical computation of $C_i^n(\underline{a})$ would then be performed with the trapezoidal rule, whose nodes are at $\xi = 0, 1$ and for which $\tilde{y}_{x_i, t_{n+1}}(0) = x_i$ and $\tilde{y}_{x_i, t_{n+1}}(\Delta t) = X_2$ are computed with the correct accuracy by the RK scheme (2.3).

For the third order RK scheme (2.4), whose nodes are at $\xi = 0, 1/2, 1$, one would then choose the approximations $\tilde{y}_{x_i, t_{n+1}}(0) = x_i$, $\tilde{y}_{x_i, t_{n+1}}(\frac{1}{2}\Delta t) = X_2$ and $\tilde{y}_{x_i, t_{n+1}}(\Delta t) = X_3$. In this special case, even if both $y_{x_i, t_{n+1}}(\xi_2 \Delta t) - X_2$ and $y_{x_i, t_{n+1}}(\xi_3 \Delta t) - X_3$ are $\mathcal{O}(\Delta x^2)$, these errors cancel each other out when computing the linear combination of the Simpson's quadrature rule, resulting in a third order accuracy for the approximation of $C_i^n(\underline{a})$. For more general RK processes, this issue can be overcome by resorting to the continuous extension [Zen86] to compute $\tilde{y}_{x_i, t_{n+1}}(\xi)$ with the proper accuracy.

To compute the solution of (2.1), we employ tabulation on a coarse grid in A , followed by a Nelder-Mead algorithm, adjusted so that no vertex of the simplices can exit the compact set A . At each step of the minimization we need to evaluate the reconstruction at the feet of the characteristics $y_i^n(\underline{a})$ for each node x_i and for each discrete control \underline{a} . Thus an efficient and accurate reconstruction operator is crucial to obtain a robust and fast numerical scheme. Since (2.1) has in general nonsmooth solutions, standard high order interpolation give rise to oscillations in the numerical solution. [CFR06], a WENO reconstruction has been applied to overcome this problem. The CWENO approach, instead, is more efficient when many evaluations of the reconstruction in each given cell are required. For this reason, we propose to apply CWENO interpolation within our semi-Lagrangian scheme (2.1).

3 CWENO reconstruction

We recall here the definition of the CWENO and CWENOZ operators, following the presentation of [CPSV18, CSV19]; in particular, despite the present finite-difference setting in place of the finite-volume one, we will still be able to exploit the general theorems for the accuracy of the reconstructions on smooth solutions proven in the aforementioned papers.

For a point $x \in \mathbb{R}^d$, let Ω be the grid cell containing it and \mathcal{S}_Ω be the set of its vertices. In order to achieve better than first order accuracy, we need to consider stencils $\mathcal{S} \supset \mathcal{S}_\Omega$. We associate to any \mathcal{S} a polynomial $P_{\mathcal{S}}^{(r)}(x) \in \mathbb{P}_d^r$ which interpolates the data in \mathcal{S} , i.e. such that $P_{\mathcal{S}}^{(r)}(x_j) = u_j \forall j \in \mathcal{S}$. Larger symmetric stencils will define highly accurate interpolators, which however would be very oscillatory when the data in \mathcal{S} represent a non smooth function. Instead, polynomials associated to smaller stencils, biased in a specific direction, could avoid the discontinuities in the data.

The general idea of CWENO and CWENOZ reconstruction is to blend, in a nonlinear and data-dependent fashion, a high order accurate interpolating polynomial with a set of lower order ones to produce an essentially non-oscillatory reconstruction polynomial for the cell Ω . This can be later evaluated at any point in $x \in \Omega$ with negligible cost.

The nonlinear selection or blending of polynomials relies on oscillation indicators $I[P]$, which are in general scalar quantities associated to a polynomial P , designed in such a way that $I[P] \rightarrow 0$ under grid refinement, if P is associated to smooth data, and $I[P] \asymp 1$, in presence of a discontinuity in the stencil \mathcal{S} . In this work we rely on the classical Jiang–Shu oscillation indicators [JS96], suitably modified to accommodate for the regularity of the solution of HJB problems under consideration [JP00, FPT20b].

We recall now the definition of the CWENO and CWENOZ reconstructions given in [CSV19].

Definition 3.1 *Given a stencil \mathcal{S}_{opt} , including \mathcal{S}_Ω , let $P_{opt} \in \mathbb{P}_n^G$ (optimal polynomial) be the polynomial of degree G , associated to \mathcal{S}_{opt} . Further, let P_1, P_2, \dots, P_m be a set of $m \geq 1$ polynomials of degree g with $g < G$, associated to substencil \mathcal{S}_k such that $\mathcal{S}_\Omega \subset \mathcal{S}_k \subset \mathcal{S}_{opt} \forall k = 1, \dots, m$. Let also $\{d_k\}_{k=0}^m$ be a set of strictly positive real coefficients such that $\sum_{k=0}^m d_k = 1$.*

The CWENO and CWENOZ operators compute a reconstruction polynomial

$$\begin{aligned} P_{rec}^{CW} &= \text{CWENO}(P_{opt}, P_1, \dots, P_m) \in \mathbb{P}_n^G, \\ P_{rec}^{CWZ} &= \text{CWENOZ}(P_{opt}, P_1, \dots, P_m) \in \mathbb{P}_n^G, \end{aligned} \quad (3.1)$$

as follows:

1. First, introduce the polynomial P_0 defined as

$$P_0(x) = \frac{1}{d_0} \left(P_{opt}(x) - \sum_{k=1}^m d_k P_k(x) \right) \in \mathbb{P}_n^G; \quad (3.2)$$

2. compute suitable regularity indicators

$$I_0 = I[P_{opt}], \quad I_k = I[P_k], \quad k \geq 1; \quad (3.3)$$

3. compute the nonlinear coefficients $\{\omega_k\}_{k=0}^m$ or $\{\omega_k^Z\}_{k=0}^m$ as

(a) CWENO operator: for $k = 0, \dots, m$,

$$\alpha_k = \frac{d_k}{(I_k + \epsilon)^l}, \quad \omega_k^{CW} = \frac{\alpha_k}{\sum_{i=0}^m \alpha_i}, \quad (3.4)$$

(b) CWENOZ operator: for $k = 0, \dots, m$,

$$\alpha_k^Z = d_k \left(1 + \left(\frac{\tau}{I_k + \epsilon} \right)^l \right), \quad \omega_k^{CWZ} = \frac{\alpha_k^Z}{\sum_{i=0}^m \alpha_i^Z}, \quad (3.5)$$

where ϵ is a small positive quantity, $l \geq 1$, and, in the case of CWENOZ, τ is a global smoothness indicator;

4. finally, define the reconstruction polynomial as

$$P_{rec}^{CW}(x) = \sum_{k=0}^m \omega_k^{CW} P_k(x) \in \mathbb{P}_n^G, \quad (3.6)$$

$$P_{rec}^{CWZ}(x) = \sum_{k=0}^m \omega_k^{CWZ} P_k(x) \in \mathbb{P}_n^G. \quad (3.7)$$

Note that the reconstruction polynomial defined in (3.6) and in (3.7) can be evaluated at any point in the computational cell Ω at a very low computational cost and this happens because the reconstruction procedure, in both cases, starts with the definition of the linear coefficients $\{d_k\}_{k=0}^m$ that do not depend on the reconstruction point. Therefore, the nonlinear coefficients given by (3.4) and (3.5) are computed once per cell and not once per reconstruction point, as in the standard WENO. We also remark that, since every polynomial taking place in the reconstruction procedures is required to satisfy the interpolation constraint on \mathcal{S}_Ω , then also P_{rec}^{CW} and P_{rec}^{CWZ} satisfy the same constraint on the vertices of Ω .

The accuracy and non-oscillatory properties of CWENO and CWENOZ schemes are guaranteed by the dependence of their nonlinear weights (3.4) and (3.5) on the regularity indicators I_k . On smooth data, the nonlinear weights are driven sufficiently close to the optimal ones, so that $P_{rec} \approx P_{opt}$ and the reconstruction reaches the optimal order of accuracy $G + 1$. On the other hand, when a discontinuity is present in \mathcal{S}_{opt} , both $I_0 \asymp 1$ and at least one $I_{\hat{k}} \asymp 1$ for some $\hat{k} \in \{1, \dots, m\}$. Then the formulas (3.4) and (3.5) for the nonlinear weights will ensure that $\omega_0 \approx 0$ and $\omega_{\hat{k}} \approx 0$ for all \hat{k} such that $P_{\hat{k}}$ would bring oscillations in the reconstruction. The reconstruction polynomial will then be a linear combination of all polynomials of degree g that are not affected by the discontinuity; the accuracy of the reconstruction thus reduces to $g + 1$, but spurious oscillations would be tamed.

3.1 One spatial dimension

Let us describe the reconstruction for any point x in the cell $\Omega = [x_j, x_{j+1}]$, so that $\mathcal{S}_\Omega = \{j, j+1\}$. We consider $\mathcal{S}_{opt} = \{j-1, j, j+1, j+2\}$ and introduce the optimal cubic polynomial $P_{opt}(x) = Q(x) = \sum_{i=0}^3 z_i [(x - x_j)/\Delta x]^i$ that interpolates the data $u_{j-1}, u_j, u_{j+1}, u_{j+2}$ at the nodes $x_{j-1}, x_j, x_{j+1}, x_{j+2}$. Next, we consider two parabolas $P_L(x)$ and $P_R(x)$ that interpolate only the data u_{j-1}, u_j, u_{j+1} and, respectively, u_j, u_{j+1}, u_{j+2} .

The reconstruction operators thus compute

$$\begin{aligned} P_{rec}^{CW} &= \text{CWENO}(Q, P_L, P_R) \in \mathbb{P}_1^3, \\ P_{rec}^{CWZ} &= \text{CWENOZ}(Q, P_L, P_R) \in \mathbb{P}_1^3. \end{aligned} \quad (3.8)$$

For any polynomial, its oscillation indicator is defined as

$$I[P] = \sum_{\alpha \geq 2} \Delta x^{2\alpha-3} \int_{x_j}^{x_{j+1}} \left(\frac{d^{(\alpha)} P}{dx^\alpha} \right)^2 dx. \quad (3.9)$$

The above definition is similar to the classical definition of the oscillation indicators for the WENO reconstruction as given in [JS96], except that the first derivative is not included in the sum. This choice is the appropriate one for Hamilton–Jacobi equations, whose solution can be at worst continuous with kinks, see [JP00], and ensures that at worst $I[P] = \mathcal{O}(1)$.

Let $P(x) = \sum_{i=0}^3 z_i [(x - x_j)/\Delta x]^i$ be a polynomial of degree up to 3. Its indicator (3.9) can be written as a quadratic form of its coefficients given by

$$I[P] = \frac{1}{\Delta x^2} (4z_2^2 + 12z_2z_3 + 48z_3^2)$$

or equivalently, denoting with \vec{z} the vector of coefficients,

$$I[P] = \frac{1}{\Delta x^2} \vec{z}^T M \vec{z}, \quad \text{with} \quad M = \begin{pmatrix} 0 & 0 & 0 & 0 \\ 0 & 0 & 0 & 0 \\ 0 & 0 & 4 & 6 \\ 0 & 0 & 6 & 48 \end{pmatrix}. \quad (3.10)$$

Denoting by U the vector of data $(u_{j-1}, u_j, u_{j+1}, u_{j+2})^T$, since the coefficients of the polynomial linearly depends on U , we can express the regularity indicators also as a quadratic form on the data being interpolated. More precisely, the vector of coefficients \vec{z} can be expressed as $\vec{z} = V^{-1}U$, where V^{-1} is the inverse of the Vandermonde matrix. Thus, in the one-dimensional case, one obtains that the matrices of the quadratic forms expressed in terms of U scale again globally as $1/\Delta x^2$:

$$I[Q] = \frac{1}{\Delta x^2} U^T A_Q U, \quad I[P_k] = \frac{1}{\Delta x^2} U^T A_k U \quad (k = L, R). \quad (3.11)$$

In our case, we get

$$A_Q = \begin{pmatrix} 4/3 & -7/2 & 3 & -5/6 \\ -7/2 & 10 & -19/2 & 3 \\ 3 & -19/2 & 10 & -7/2 \\ -5/6 & 3 & -7/2 & 4/3 \end{pmatrix},$$

$$A_L = \begin{pmatrix} 1 & -2 & 1 & 0 \\ -2 & 4 & -2 & 0 \\ 1 & -2 & 1 & 0 \\ 0 & 0 & 0 & 0 \end{pmatrix}, \quad A_R = \begin{pmatrix} 0 & 0 & 0 & 0 \\ 0 & 1 & -2 & 1 \\ 0 & -2 & 4 & -2 \\ 0 & 1 & -2 & 1 \end{pmatrix}.$$

The CWENO reconstruction applied in the numerical tests of this paper is then defined by choosing linear coefficients $d_L = d_R = 1/8$ and $d_0 = 3/4$, $l = 2$ and $\epsilon = \Delta x^2$ in the above construction.

For the optimal definition of the CWENOZ reconstruction, in order to exploit the results of [CSV19], we need to study the Taylor expansions of the indicators centered at the point $x_0 = (x_j + x_{j+1})/2$, namely the center of the reconstruction cell Ω . They are given by

$$\begin{aligned} I[P_L] &= B - u''(x_0)u'''(x_0)\Delta x^3 + \frac{1}{4}u'''(x_0)^2\Delta x^4 + \mathcal{O}(\Delta x^5), \\ I[P_R] &= B + u''(x_0)u'''(x_0)\Delta x^3 + \frac{1}{4}u'''(x_0)^2\Delta x^4 + \mathcal{O}(\Delta x^5), \\ I[P_L] &= B + \frac{13}{12}u'''(x_0)^2\Delta x^4 + \mathcal{O}(\Delta x^5), \end{aligned} \quad (3.12)$$

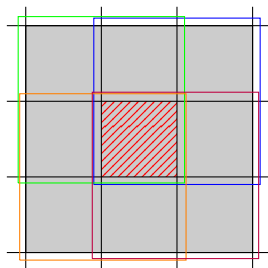


Figure 1: Stencils of the two-dimensional CWENO and CWENOZ reconstructions. The red hatched region represents the cell $\Omega_{i,j}$ in which we compute the reconstruction. The vertices of \mathcal{S}_{opt} are enclosed in the grey shaded region, while the stencils for the low degree polynomials are enclosed in the coloured squares: blue, green, orange and purple, respectively for the north-east, north-west, south-west and south-east polynomial.

where $B = u''(x_0)^2 \Delta x^2$. Thus, defining

$$\tau = \left| 2\mathbb{I}[Q] - \mathbb{I}[P_L] - \mathbb{I}[P_R] \right|, \quad (3.13)$$

all terms up to $\mathcal{O}(\Delta x^3)$ cancel. Note that this is the optimal definition of τ since it is never possible to cancel all the $\mathcal{O}(\Delta x^4)$ terms in a convex combination of the three indicators. The hypotheses of Theorem 24 in [CSV19] hold and we can guarantee the optimal order of accuracy of the CWENOZ reconstruction for $l = 2$.

3.2 Two spatial dimensions

In two space dimensions, we will not rely on dimensional splitting. Such an approach would in fact nullify the advantages of a fast evaluation of the reconstruction polynomial on a large number of arbitrary points in the reconstruction cell. Our reconstruction will instead generate a polynomial of two variables, like it is done in [SCR16, CS19] for Cartesian meshes or in general mesh settings [ZQ20, DBSR17, BGF20].

Let Ω be the cell of the Cartesian grid containing the reconstruction point x . The setup of the stencils for the reconstruction is illustrated in Fig. 1: the cell Ω , with corners (x_i, y_j) and (x_{i+1}, y_{j+1}) , is hatched in red and the reconstruction stencil is shaded in gray.

The reconstruction operators compute

$$\begin{aligned} P_{\text{rec}}^{CW} &= \text{CWENO}(Q^{(3)}; Q_{\text{ne}}^{(2)}, Q_{\text{se}}^{(2)}, Q_{\text{sw}}^{(2)}, Q_{\text{nw}}^{(2)}) \in \mathbb{P}_1^3 \otimes \mathbb{P}_1^3, \\ P_{\text{rec}}^{CWZ} &= \text{CWENOZ}(Q^{(3)}; Q_{\text{ne}}^{(2)}, Q_{\text{se}}^{(2)}, Q_{\text{sw}}^{(2)}, Q_{\text{nw}}^{(2)}) \in \mathbb{P}_1^3 \otimes \mathbb{P}_1^3, \end{aligned} \quad (3.14)$$

with the optimal polynomial set to the bicubic polynomial interpolating the 16 data points in the square with corners (x_{i-1}, y_{j-1}) and (x_{i+2}, y_{j+2}) enclosed in the grey shaded region of Fig 1. The other four polynomials are the biquadratic polynomials that interpolate the four 3×3 substencils in the north-east, south-east, south-west and north-west directions, as illustrated in Fig. 1, named \mathcal{S}_{ne} , \mathcal{S}_{nw} , \mathcal{S}_{sw} and \mathcal{S}_{se} , respectively. In particular, the blue box with vertices (x_i, y_j) and (x_{i+2}, y_{j+2}) encloses \mathcal{S}_{ne} , the green box with vertices (x_{i-1}, y_j) and (x_{i+1}, y_{j+2}) encloses \mathcal{S}_{nw} , the orange box with vertices (x_{i-1}, y_{j-1}) and (x_{i+1}, y_{j+1}) encloses \mathcal{S}_{sw} and the purple box with vertices (x_i, y_{j-1}) and (x_{i+2}, y_{j+1}) encloses \mathcal{S}_{se} . The basis for bicubic and

biquadratic polynomials are defined by tensorization and are thus respectively given by

$$\begin{aligned}\mathcal{B}_3 &= \{1, \hat{x}, \hat{y}, \hat{x}^2, \hat{x}\hat{y}, \hat{y}^2, \hat{x}^3, \hat{x}^2\hat{y}, \hat{x}\hat{y}^2, \hat{y}^3, \hat{x}^3\hat{y}, \hat{x}^2\hat{y}^2, \hat{x}\hat{y}^3, \hat{x}^3\hat{y}^2, \hat{x}^2\hat{y}^3, \hat{x}^3\hat{y}^3\}, \\ \mathcal{B}_2 &= \{1, \hat{x}, \hat{y}, \hat{x}^2, \hat{x}\hat{y}, \hat{y}^2\},\end{aligned}$$

where $\hat{x} = (x - x_i)/\Delta x$ and $\hat{y} = (y - y_j)/\Delta y$.

The oscillation indicators are defined as

$$I[P] = \sum_{|\bar{\alpha}| \geq 2} \Delta^{2|\bar{\alpha}|-4} \int_{\Omega_{i,j}} \left[\frac{\partial P}{\partial x^{\alpha_1} \partial y^{\alpha_2}} \right]^2 dx dy \quad (3.15)$$

where Δ is the diameter of the cell $\Omega_{i,j}$. These indicators are inspired to the classical ones of [HS99], but the powers of Δ appearing in (3.15) have been adjusted for the expected regularity of the solution to Hamilton–Jacobi equations. In particular the scaling $\Delta^{2|\bar{\alpha}|-4}$ is a generalization to two space dimensions of the choice of [JP00]; it is introduced so that $I[P] \asymp 1$ for functions with discontinuous first derivative and $I[P] = \mathcal{O}(\Delta^2)$ on regular solutions. A detailed discussion of this scaling can be found in [FPT20b].

Denoting with \vec{z} the vector of coefficients along the basis \mathcal{B}_3 of a generic polynomial in two variables of degree up to 3, and considering a uniform grid of size Δx , its oscillation indicator can be expressed as

$$I[P] = \frac{1}{\Delta x^2} \vec{z}^T M \vec{z} \quad (3.16)$$

for a 16×16 matrix M . We point out that in the case of Cartesian but uneven grids, there would still be a global factor inversely proportional to the local grid size, but matrix M would also depend on the aspect ratios and on the ratios of sizes of nearby cells.

Consider now the stencil of the reconstruction given by $\{(x_{i-1+k}, y_{j-1+l})\}_{\substack{l=0,\dots,3 \\ k=0,\dots,3}}$ and denote by U the corresponding vector of values $\{(u_{i-1+k}, y_{j-1+l})\}_{\substack{l=0,\dots,3 \\ k=0,\dots,3}}$ with a prescribed ordering, e.g. lexicographic. Thanks to the linear relation among the coefficients \vec{z} and the data vector U , the regularity indicators can be expressed in the form

$$I[Q] = \frac{1}{\Delta x^2} U^T A_Q U, \quad I[Q_k] = \frac{1}{\Delta x^2} U^T A_k U \quad (k = \text{ne, se, sw, nw}). \quad (3.17)$$

The matrices A_Q and A_k will in general depend on the local aspect ratio of cells and on the neighbours size ratio.

The CWENO reconstruction is then defined by choosing linear coefficients $d_k = 1/16$ and $d_0 = 1 - \sum_k d_k$ with $k \in \{\text{ne, se, sw, nw}\}$, $l = 2$ and $\epsilon = \Delta x^2$.

The CWENOZ reconstruction is computed choosing $l = 2$ and

$$\tau = \left| 4I[Q^{(3)}] - I[Q_{\text{ne}}^{(2)}] - I[Q_{\text{se}}^{(2)}] - I[Q_{\text{sw}}^{(2)}] - I[Q_{\text{nw}}^{(2)}] \right| \quad (3.18)$$

in order to guarantee the optimal order of accuracy of the CWENOZ reconstruction, see [CSV19, Theorem 24]. In fact, computing the Taylor expansions of the indicators centered at the center of the cell Ω , one gets, for smooth enough data,

$$\begin{aligned}I[Q_{\text{ne}}^{(2)}] &= B + 2u_{xx}u_{xxx}\Delta x^3 + 2u_{yy}u_{yyy}\Delta x^3 + \mathcal{O}(\Delta x^4), \\ I[Q_{\text{nw}}^{(2)}] &= B - 2u_{xx}u_{xxx}\Delta x^3 + 2u_{yy}u_{yyy}\Delta x^3 + \mathcal{O}(\Delta x^4), \\ I[Q_{\text{sw}}^{(2)}] &= B - 2u_{xx}u_{xxx}\Delta x^3 - 2u_{yy}u_{yyy}\Delta x^3 + \mathcal{O}(\Delta x^4), \\ I[Q_{\text{se}}^{(2)}] &= B + 2u_{xx}u_{xxx}\Delta x^3 - 2u_{yy}u_{yyy}\Delta x^3 + \mathcal{O}(\Delta x^4), \\ I[Q^{(3)}] &= B + \mathcal{O}(\Delta x^4)\end{aligned} \quad (3.19)$$

where $B = (u_{xx}^2 + u_{xy}^2 + u_{yy}^2)\Delta x^2$. Therefore, the coefficients chosen for the definition of τ in (3.18), cancel all terms up to $\mathcal{O}(\Delta x^3)$, thus ensuring that the hypotheses of [CSV19, Theorem 24] hold.

4 Convergence

The convergence analysis will be carried out in one space dimension, and follow the guidelines of [Fer02, CFR06], which will be briefly reviewed here. Assume that equation (1.1) is posed on \mathbb{R} in the simplified form

$$\begin{cases} v_t(t, x) + H(Dv(t, x)) = 0 & t, x \in (0, T) \times \mathbb{R}, \\ v(0, x) = v_0(x), & x \in \mathbb{R}. \end{cases} \quad (4.1)$$

Also assume that the Hamiltonian function H is a $W^{2,\infty}$ function and that

$$H''(p) \geq m_H > 0. \quad (4.2)$$

The convexity assumption (4.2) implies, by the Fenchel duality formula, that $H(\cdot)$ can always be written in the form

$$H(Dv(t, x)) = \sup_{a \in \mathbb{R}} \{a Dv(t, x) - H^*(a)\},$$

where H^* denotes the Legendre transform of H . Moreover, the restriction of the supremum can be limited to a suitable compact set A , so that problem (4.1) can be recast in the case of a Hamiltonian of the form (1.3), by setting $f_D(t, x, a) = -a$ and $f_C(t, x, a) = H^*(a)$.

The key assumption is that for any Lipschitz continuous function $v(x)$, once defined the sequence $V = \{v_j\}_j = \{v(x_j)\}_j$, the interpolation operator $R[V]$ satisfies $R[V](x_k) = v(x_k)$ and, for some constant $C < 1$:

$$|R[V](x) - R_1[V](x)| \leq C \max_{x_k \in U(x)} |v_{k+1} - 2v_k + v_{k-1}| \quad (4.3)$$

where by $R_1[V]$ we denote the \mathbb{P}_1 (i.e., piecewise linear) interpolation on the sequence V , and by $U(x) = (x - h_- \Delta x, x + h_+ \Delta x)$ the interval containing the stencil of the reconstruction $R[V](x)$. For example, in our case the reconstruction is performed taking two nodes on the left and two nodes on the right of the point x , so that $h_- = h_+ = 2$.

Under such assumptions it is possible (see [Fer02]) to prove the following

Theorem 4.1 *Consider the scheme (2.1) applied to equation (4.1), and assume that (4.2) and (4.3) hold, that $\Delta x = \mathcal{O}(\Delta t^2)$ and that v_0 is Lipschitz continuous. Then, the numerical solution $U^n = \{u_j^n\}_j$ (with u_j^n defined by (2.1)) satisfies*

$$\|R[U^n] - v(n\Delta t)\|_\infty \rightarrow 0$$

(where v is the solution of (4.1)) for $0 \leq n \leq T/\Delta t$, as $\Delta t \rightarrow 0$.

It is proved in [Fer02] that condition (4.3) is satisfied for Lagrange reconstructions up to the fifth order, if the reconstruction stencil includes the interval $[x_j, x_{j+1}]$. Since WENO interpolation is performed by taking a convex combination of polynomials which satisfy (4.3) up to the degree 5 for the partial polynomials (and therefore, up to the degree 9 for the global interpolant), this fact is used in [CFR06] to obtain convergence via Theorem 4.1. This essentially boils down to

proving that the all the function appearing in the convex combination defining R satisfy (4.3), and we plan to apply the same principle here.

In the case of CWENO, once set $d_L = d_R = d$ and recast P_0 as

$$P_0(x) = \frac{1}{1-2d}(Q(x) - dP_L(x) - dP_R(x)),$$

we estimate the left-hand side of (4.3) as

$$\begin{aligned} |R - R_1| &= |\omega_0 P_0 + \omega_L P_L + \omega_R P_R - R_1| \\ &= |\omega_0(P_0 - R_1) + \omega_L(P_L - R_1) + \omega_R(P_R - R_1)| \\ &\leq \max\{|P_0 - R_1|, |P_L - R_1|, |P_R - R_1|\}, \end{aligned}$$

where the identity $\omega_0 + \omega_L + \omega_R = 1$ has been used twice. As it has been proved in [Fer02], both P_L and P_R satisfy (4.3). It remains then to check that the same property holds for P_0 . We have:

$$\begin{aligned} |P_0 - R_1| &= \left| \frac{1}{1-2d}(Q - dP_L - dP_R) - R_1 \right| \\ &= \left| \frac{1}{1-2d}(Q - dP_L - dP_R + (2d-1)R_1) \right| \\ &= \left| \frac{1}{1-2d}((Q - R_1) - d(P_L - R_1) - d(P_R - R_1)) \right| \\ &\leq \frac{1}{1-2d}|Q - R_1| + \frac{d}{1-2d}|P_L - R_1| + \frac{d}{1-2d}|P_R - R_1|. \end{aligned}$$

Denoting now by C_r the constant appearing in (4.3) for the specific case of an interpolation of degree r , we finally obtain an estimate in the form

$$|P_0 - R_1| \leq \left(\frac{1}{1-2d}C_3 + \frac{2d}{1-2d}C_2 \right) \max_{x_k \in U(x)} |v_{k+1} - 2v_k + v_{k-1}|.$$

As proved in [Fer02], $C_2 = 1/8$ and $C_3 \approx 0.2533$; then, it turns out that (4.3) is satisfied for $d \lesssim 0.332$, and therefore, with this additional condition, all the assumptions of Theorem 4.1 are satisfied, and the scheme (2.1) converges to the viscosity solution of (4.1).

We point out that our choice of $d_0 = 3/4$, i.e. $d = d_L = d_R = 1/8$ in the CWENO and CWENOZ reconstructions employed in this paper fully satisfies the above requirement.

5 Numerical tests

Here, we present some numerical tests in order to assess the performance of the schemes proposed in this paper. In particular, we focus on the expected accuracy of the schemes, considering the L^1 -norm of the error, and the computational times, reported in seconds. In particular we will compare the SL schemes using the CWENO and CWENOZ reconstructions of §3 and those employing the dimensionally-split WENO approach of [CFR06].

In order to account for bounded domains, we consider either periodic boundary conditions or extrapolation technique. It is noteworthy that in all the numerical tests where extrapolation is applied, the solution has a compact support, or the boundary of the numerical domain is entirely of outflow type. In both cases, these conditions ensure no loss in accuracy in the numerical treatment of the boundary. In all tests, unless otherwise stated, we employ an extrapolation

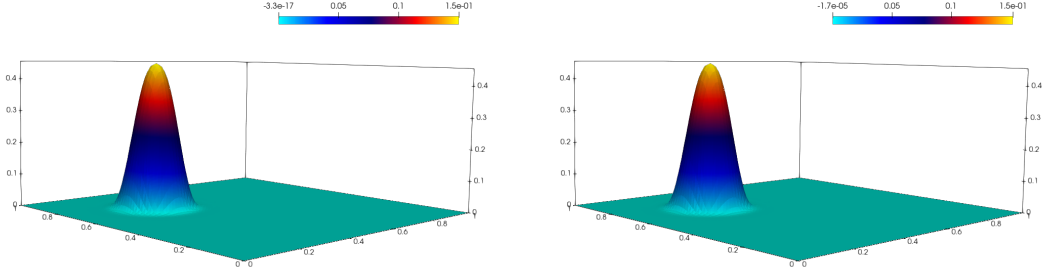


Figure 2: Initial condition (left) and numerical solution at $T = 1$ (right) for Test 1 computed with CWENOZ reconstruction and $N = 81$.

technique. For more general boundary conditions, we refer to [CCDS23] for approximations of Neumann-type boundary conditions and to [BCCF21] for a second order accurate treatment of Dirichlet boundary conditions.

Although the convergence analysis requires a relation $\Delta x = \mathcal{O}(\Delta t^2)$ between the time and space steps, in practice, smaller time steps are also allowed. Heuristically, assuming exact minimization, and supposing a third order time discretization is used, then the consistency error is given by

$$\mathcal{T}(\Delta t, \Delta x) = \mathcal{O}\left(\Delta t^3 + \frac{\Delta x^q}{\Delta t}\right),$$

where q is the order of the interpolation in space. For smooth solutions, the choice $\Delta t = \mathcal{O}(\Delta x^{q/4})$ optimizes this error and leads to a numerical convergence rate of $3q/4$.

In particular, choosing $q = 4$ (i.e., a cubic reconstruction), we obtain

$$\mathcal{T}(\Delta t, \Delta x) = \mathcal{O}\left(\Delta t^3 + \frac{\Delta x^4}{\Delta t}\right),$$

which results in an overall order of 3 for the choice $\Delta t = \mathcal{O}(\Delta x)$. In the particular case where the Hamiltonian is independent of (t, x) , the characteristics solving problem (1.2) are affine, and even a first order time discretization computes them exactly, reducing the consistency error to

$$\mathcal{T}(\Delta t, \Delta x) = \mathcal{O}\left(\frac{\Delta x^q}{\Delta t}\right).$$

In this case, the larger the time step, the smaller the consistency errors.

In what follows N indicates the number of grid points per direction, so that $\Delta x \sim 1/N$. The tests have been performed on the cluster Galileo 100 hosted at CINECA¹.

Test 1: Passive advection. As a first benchmark problem, we consider the uniform rotation of a scalar field in two space dimensions, expressed by the linear transport equation

$$v_t - f_D \cdot Dv = 0,$$

¹<https://www.hpc.cineca.it/systems/hardware/galileo100/>

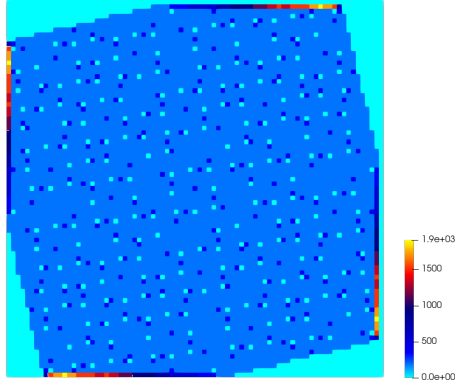


Figure 3: Reconstructions count for Test 1 in the final time step on a grid of 81×81 points.

N	WENO		CWENO		CWENOZ	
	L^1 -err	L^1 -ord	L^1 -err	L^1 -ord	L^1 -err	L^1 -ord
21×21	$2.97e - 03$		$2.98e - 03$		$2.98e - 03$	
41×41	$5.46e - 04$	2.44	$4.88e - 04$	2.61	$4.84e - 04$	2.62
81×81	$1.24e - 04$	2.13	$8.18e - 05$	2.57	$7.85e - 05$	2.62
161×161	$2.34e - 05$	2.41	$1.22e - 05$	2.75	$1.12e - 05$	2.80
321×321	$3.92e - 06$	2.58	$1.72e - 06$	2.82	$1.49e - 06$	2.92
641×641	$6.11e - 07$	2.68	$2.27e - 07$	2.92	$1.79e - 07$	3.05
1281×1281	$8.87e - 08$	2.78	$2.92e - 08$	2.96	$2.06e - 08$	3.12

Table 1: Errors at time $T = 1$ for Test 1, WENO, CWENO and CWENOZ schemes.

grid	WENO	CWENO		CWENOZ	
	CPU time	CPU time	% gain	CPU time	% gain
21×21	$1.05e + 00$	$7.22e - 01$	31.21	$1.01e - 01$	90.36
41×41	$1.10e + 00$	$1.06e + 00$	3.39	$7.20e - 01$	34.25
81×81	$7.84e + 00$	$5.42e + 00$	30.87	$5.46e + 00$	30.39
161×161	$6.19e + 01$	$4.36e + 01$	29.51	$4.37e + 01$	29.35
321×321	$4.86e + 02$	$3.38e + 02$	30.47	$3.36e + 02$	30.95
641×641	$3.87e + 03$	$2.70e + 03$	30.31	$2.67e + 03$	30.99
1281×1281	$3.09e + 04$	$2.12e + 04$	31.25	$2.12e + 04$	31.32

Table 2: CPU times for Test 1, WENO and CWENO schemes.

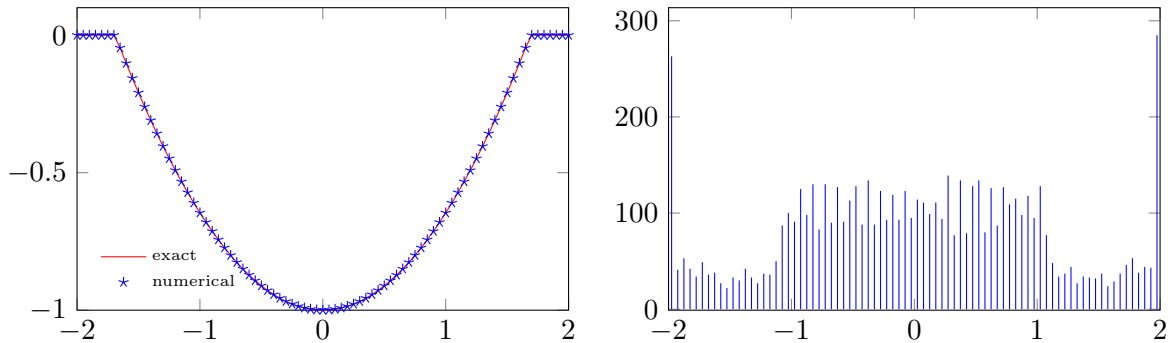


Figure 4: Left: the exact solution of Test 2 in red and the numerical one in blue computed with a third order CWENOZ reconstruction and $N = 81$. Right: reconstructions count in the last time step.

which is included in our setting by choosing in (1.3) $A = \emptyset$ and $f_C = 0$. The speed of propagation is given by the vector field $f_D = (-2\pi(x_2 - 0.5), 2\pi(x_1 - 0.5))$ in the square domain $[0, 1] \times [0, 1]$. We choose as initial condition the globally \mathcal{C}^2 function

$$v(0, x) = v_0(r) = M \left(1 + \frac{r^3}{R^3} \left(-1 + 3 \frac{r-R}{R} \left(1 - 2 \frac{r-R}{R} \right) \right) \right)$$

with $r = |x - (0.3, 0.7)|$ and parameters $M = 0.15$, $R = 0.15$. Numerical solutions are computed at the final time $T = 1$, using a relationship of $\Delta t = 3\Delta x$ among the discretization steps. Since the advection is rigid, the exact solution at final time coincides with the initial condition. We point out that the characteristic lines are not affine, therefore we use the third order RK scheme and a third order reconstruction scheme as described in section §2 and §3, respectively. Plots of the initial data and of the numerical solution are shown in Fig. 2.

As expected, since the transport is rigid and the initial data is globally \mathcal{C}^2 , all the schemes (WENO, CWENO and CWENOZ) yield solutions converging with the same order, see Table 1. However, central reconstructions are more accurate with respect to the traditional WENO one; in particular, CWENOZ achieves the best results: its errors are about one-half than those of WENO. The fundamental difference among the schemes is in their computational costs, which are shown in Table 2. The high number of reconstructions performed in each cell (see Fig. 3) allows the CWENO and CWENOZ to save about the 30% of time. This happens because Central WENO reconstructions compute their nonlinear coefficients only once per cell instead of once per reconstruction point. Looking at Fig. 3, note in particular that the high number of reconstructions performed near the boundary is related to the boundedness of the domain: in fact, except for the case of periodic boundary conditions, each time a foot of a characteristic falls outside the domain, it is projected back in the first cell near the boundary in order to compute the reconstruction.

Test 2: One-dimensional semi-concave data. This test deals with the HJ equation

$$\begin{cases} v_t(t, x) + \frac{1}{2} |\partial_x v(t, x)|^2 = 0 \\ v(0, x) = v_0(x) = \min(-\cos(\pi x/2), 0), \end{cases} \quad (5.1)$$

in the domain $[-2, 2]$, with homogeneous boundary conditions, which are treated using the extrapolation technique. The approximate solution is computed, at $T = 1$, with $\Delta t = 10\Delta x$,

N	WENO		CWENO		CWENOZ	
	L^1 -err	L^1 -ord	L^1 -err	L^1 -ord	L^1 -err	L^1 -ord
81	$3.56e - 06$		$2.24e - 06$		$1.78e - 06$	
161	$2.83e - 07$	3.65	$1.80e - 07$	3.64	$1.44e - 07$	3.63
321	$2.45e - 08$	3.53	$1.59e - 08$	3.50	$1.30e - 08$	3.47
641	$2.61e - 09$	3.23	$1.96e - 09$	3.02	$1.75e - 09$	2.90

Table 3: Errors at time $T = 1$ for Test 2, WENO, CWENO and CWENOZ schemes.

grid	WENO	CWENO		CWENOZ	
	CPU time	CPU time	% gain	CPU time	% gain
81	$6.19e - 03$	$4.83e - 03$	21.95	$4.86e - 03$	21.48
161	$9.79e - 03$	$8.88e - 03$	9.31	$8.64e - 03$	11.76
321	$2.74e - 02$	$2.39e - 02$	13.03	$2.39e - 02$	12.84
641	$9.42e - 02$	$7.65e - 02$	18.81	$7.68e - 02$	18.41
1281	$3.48e - 01$	$2.83e - 01$	18.65	$2.90e - 01$	16.72
2561	$1.33e + 00$	$1.10e + 00$	17.15	$1.10e + 00$	16.83
5121	$5.28e + 00$	$4.30e + 00$	18.51	$4.29e + 00$	18.77
10241	$2.09e + 01$	$1.68e + 01$	19.42	$1.68e + 01$	19.46

Table 4: CPU times for Test 2, WENO and CWENO schemes.

while the exact solution $v(t, x)$ is defined as follows:

$$v(t, x) = \min\left(0, \frac{1}{2}[a^*(t, x)]^2 + v_0(x - ta^*(t, x))\right), \quad (5.2)$$

where, for a given (t, x) , $a^*(t, x)$ represents the optimal control, which is constant along the characteristics, and it can be computed as the solution of

$$a^*(t, x) = g(t, x, a^*(t, x)) \quad (5.3)$$

with the function g defined by

$$g(t, x, a^*(t, x)) = \begin{cases} -\frac{2}{\pi t} \arcsin \frac{2a^*(t, x)}{\pi} + \frac{x}{t} & \text{if } |a^*(t, x)| \leq \frac{\pi}{2}, \\ \frac{\pi}{2} & \text{if } a^*(t, x) > \frac{\pi}{2}, \\ -\frac{\pi}{2} & \text{if } a^*(t, x) < -\frac{\pi}{2}. \end{cases} \quad (5.4)$$

For our purposes, since the exact solution of (5.3) is not available, we compute an approximate solution by using a fixed point algorithm with initial guess $a_0^*(t, x) = \frac{1}{2}x^2t$.

Since the characteristics are affine, in this test we have combined the third order spatial reconstructions with RK1 time stepping, which computes these curves exactly. Plots of the numerical and exact solutions are shown in the left panel of Figure 4 and L^1 errors are listed in Table 3. In this case too, all schemes compute approximations affected by errors of the same order but the central reconstructions turn out to be more accurate (errors are about 2/3 than the WENO case). In fact, the feet of the characteristics fall in regular regions of v at each time step, and therefore all the reconstructions are close to the optimal cubic one. Table 4 reports the computational costs of each scheme, showing an average gain of 16 – 19% for both the Central

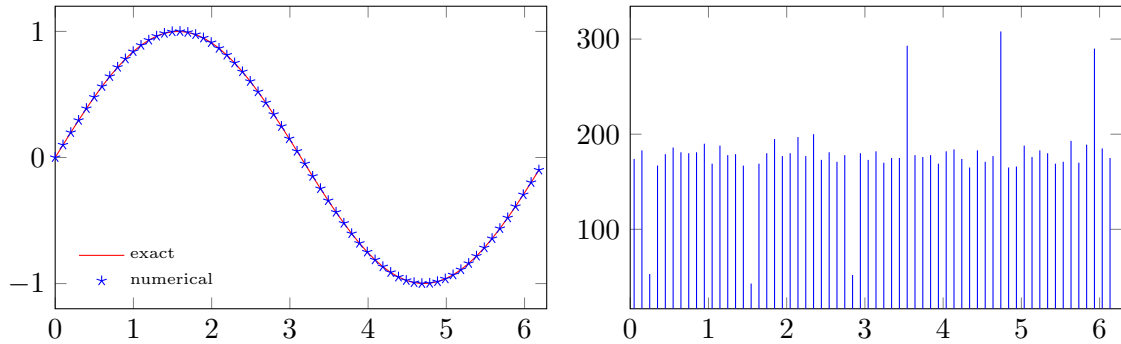


Figure 5: Left: the exact solution of Test 3 in red and the numerical one in blue computed with a third order CWENOZ scheme and $N = 63$. Right: reconstructions count in the last time step.

N	WENO		CWENO		CWENOZ	
	L^1 -err	L^1 -ord	L^1 -err	L^1 -ord	L^1 -err	L^1 -ord
126	$1.28e - 05$		$1.38e - 05$		$1.43e - 05$	
252	$1.54e - 06$	3.05	$1.65e - 06$	3.07	$1.70e - 06$	3.07
503	$1.93e - 07$	3.00	$2.03e - 07$	3.02	$2.10e - 07$	3.02
1006	$2.56e - 08$	2.91	$2.63e - 08$	2.95	$2.71e - 08$	2.95

Table 5: Errors at time $T = 1$ for Test 3, WENO, CWENO and CWENOZ schemes.

WENO reconstructions. This is again the effect of the multiple reconstructions performed in each cell (see the right panel of Figure 4, in which the number of reconstructions performed in each cell during the last time step is depicted). We point out that, as in Test 1, the high number of reconstructions computed in the first and in the last cell is related to the boundary conditions.

Test 3: One-dimensional eikonal equation. In this test, we consider the HJ equation

$$\begin{cases} v_t(t, x) + \frac{1}{2}|\partial_x v(t, x)|^2 - f(t, x) = 0 \\ v(0, x) = v_0(x), \end{cases} \quad (5.5)$$

grid	WENO	CWENO		CWENOZ	
	CPU time	CPU time	% gain	CPU time	% gain
126	$5.92e - 02$	$5.42e - 02$	8.43	$5.64e - 02$	4.81
252	$2.11e - 01$	$1.94e - 01$	8.04	$1.94e - 01$	8.05
503	$7.97e - 01$	$7.37e - 01$	7.53	$7.48e - 01$	6.05
1006	$3.13e + 00$	$2.83e + 00$	9.75	$2.87e + 00$	8.45
2011	$1.19e + 01$	$1.11e + 01$	6.67	$1.11e + 01$	6.79
4022	$4.73e + 01$	$4.27e + 01$	9.58	$4.21e + 01$	11.03
8043	$1.80e + 02$	$1.65e + 02$	8.63	$1.62e + 02$	10.02
16085	$6.96e + 02$	$6.41e + 02$	7.96	$6.38e + 02$	8.35

Table 6: CPU times for Test 3, WENO and CWENO schemes.

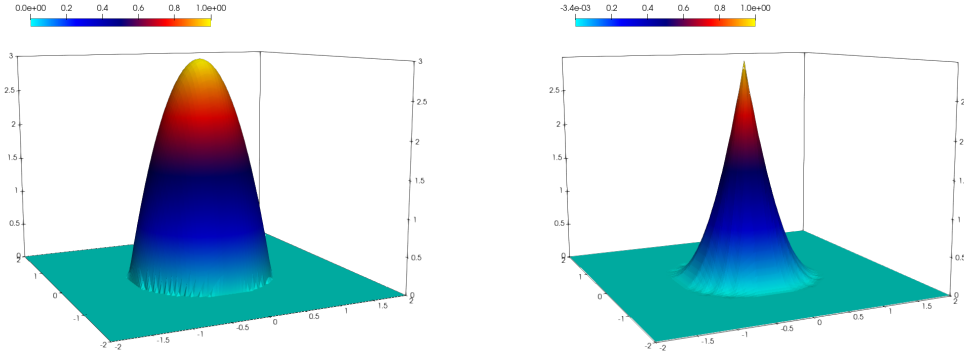


Figure 6: Test 4. Initial condition (left) and numerical solution computed with CWENO at $T = 1$ (right) with $N = 81$.

N	WENO		CWENO		CWENOZ	
	L^1 -err	L^1 -ord	L^1 -err	L^1 -ord	L^1 -err	L^1 -ord
41×41	$4.02e - 02$		$3.38e - 02$		$3.38e - 02$	
81×81	$2.25e - 02$	0.84	$1.82e - 02$	0.90	$1.81e - 02$	0.90
161×161	$1.15e - 02$	0.96	$9.01e - 03$	1.01	$8.99e - 03$	1.01
321×321	$5.56e - 03$	1.05	$4.10e - 03$	1.14	$4.09e - 03$	1.14
641×641	$2.85e - 03$	0.97	$2.03e - 03$	1.02	$2.02e - 03$	1.02

Table 7: Errors at time $T = 1$ for Test 4, WENO, CWENO and CWENOZ schemes.

with $f(t, x) = -\sin(x) + (\frac{9}{8} + \frac{t^2-3t}{2})\cos^2(x)$ and $v_0(x) = \frac{3}{2}\sin(x)$. We consider the problem in $[0, 2\pi]$ with periodic boundary conditions and compute the numerical solution at time $T = 0.5$, with $\Delta t = \Delta x$. This problem has a known exact solution given by $v(t, x) = (\frac{3}{2} - t)\sin(x)$.

In this case, characteristics are not affine and both the dynamic and the cost function explicitly depend on x and t . Therefore this is a specific test for the third order accuracy of our scheme, which depends on the use of the third order RK scheme (2.4) and on the approximation of the integral of the cost function.

Plots of the exact and of the numerical solution are shown in the left panel of Fig.5, while in the right panel the reconstruction count in the last time step is depicted. We point out that in this case, with periodic boundary conditions, there is no artificial increase in the first and in the last cell near the boundary.

Errors and computational times are listed in Tables 5 and 6. As in the previous tests, due to the regularity of the exact solution, all schemes perform almost equally when compared in terms of the error. Looking at the computational costs, the Central WENO reconstructions allow for a saving of about 6 – 10%.

Test 4: Two-dimensional semi-convex data. In this test, the HJ equation

$$\begin{cases} v_t(t, x) + \frac{1}{2}|Dv(t, x)|^2 = 0 \\ v(0, x) = v_0(x) = \max(1 - |x|^2, 0), \end{cases} \quad (5.6)$$

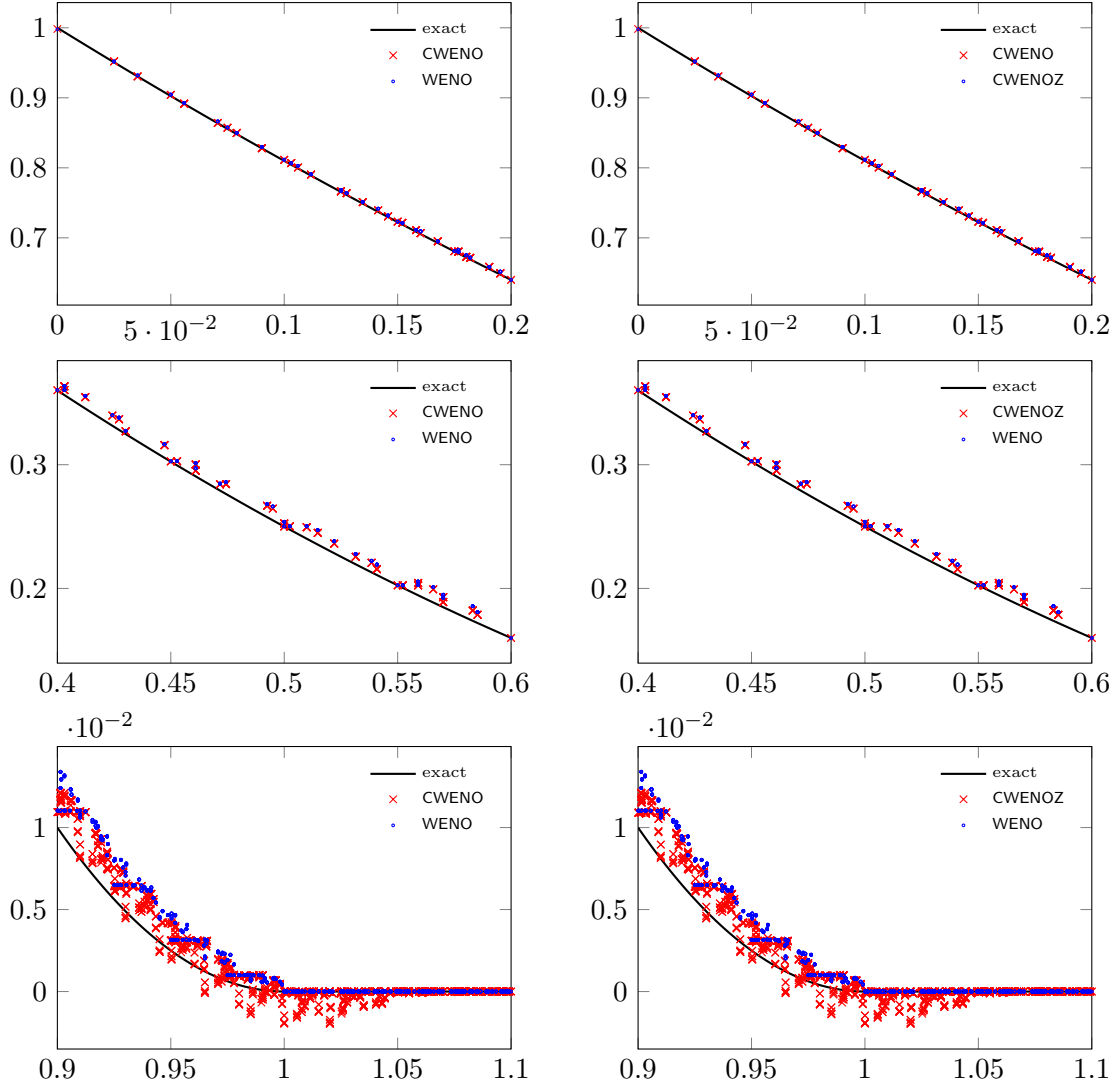


Figure 7: Test 4. Comparison of overshoots and undershoots of the numerical solutions computed with the traditional WENO scheme and with the central WENO ones on a 161×161 grid. In the left panels WENO and CWENO are compared, while in the right panels similar plots are shown for WENO and CWENOZ. The exact solution is always represented with a thick black line. First row: scatter plots of all data points with $r \in [0, 0.2]$ corresponding to the spike of the solution. Second row: scatter plots of all data points with $r \in [0.4, 0.6]$ corresponding to regular region of the solution. Third row: scatter plots of all data points with $r \in [0.9, 1.1]$ corresponding to the singular region of the initial data.

	WENO	CWENO		CWENOZ	
grid	CPU time	CPU time	% gain	CPU time	% gain
41×41	$2.88e + 00$	$1.98e + 00$	31.37	$1.96e + 00$	32.07
81×81	$2.19e + 01$	$1.54e + 01$	29.70	$1.53e + 01$	30.07
161×161	$1.72e + 02$	$1.19e + 02$	31.10	$1.18e + 02$	31.35
321×321	$1.37e + 03$	$9.38e + 02$	31.56	$9.34e + 02$	31.86
641×641	$1.09e + 04$	$7.44e + 03$	31.59	$7.51e + 03$	30.93

Table 8: CPU times for Test 4, WENO and CWENO schemes.

	WENO		CWENO		CWENOZ	
N	min	max	min	max	min	max
21×21	$-5.67e - 05$	$9.76e - 01$	$-6.08e - 03$	$9.80e - 01$	$-6.08e - 03$	$9.80e - 01$
41×41	$-4.62e - 05$	$9.89e - 01$	$-5.19e - 03$	$9.92e - 01$	$-5.19e - 03$	$9.92e - 01$
81×81	$-1.21e - 05$	$9.95e - 01$	$-3.39e - 03$	$9.96e - 01$	$-3.39e - 03$	$9.96e - 01$
161×161	$-3.45e - 06$	$9.98e - 01$	$-1.97e - 03$	$9.98e - 01$	$-1.97e - 03$	$9.98e - 01$

Table 9: Overshoots and undershoots observed in Test 4, WENO, CWENO and CWENOZ schemes.

is considered in $[-2, 2]^2$, using extrapolation techniques to treat the homogeneous boundary condition. The exact solution of this problem is known and is given, for $t \geq 1/2$, by

$$v(t, x) = \begin{cases} \frac{(|x|-1)^2}{2t} & \text{if } |x| \leq 1, \\ 0 & \text{if } |x| > 1. \end{cases} \quad (5.7)$$

We set final time $T = 0.5$ and compute the approximate solution with $\Delta t = \frac{5}{4}\Delta x$. Initial condition and final numerical solution are shown in Figure 6, while L^1 errors and CPU times are reported respectively in Tables 7 and 8.

Since in this case the feet of characteristics always fall in the singular region of the solution, we observe, as expected, that all numerical schemes are degraded to first order accuracy. From Table 7 one can see that the L^1 -norm of the error is about 30% lower for the central reconstructions, as in the previous cases. From Table 9 and Figure 7 we can see that near the kink in the solution, the central reconstructions produce larger undershoots in the flat region, while being closer to the exact solution in the nonzero region. Finally, from Table 8 one can observe that central reconstructions schemes are about 30% faster.

Test 5: Front propagation with obstacles. Last, we consider a state constrained Zermelo problem, proposed in [BFZ10], for a swimmer that has to reach a circular island at $(1, 0)$, facing a non-constant current flowing in the horizontal direction. Two obstacles are placed in the domain, near the target.

More precisely, to consider the minimum time problem the running cost $f_C(t, x, a)$ is set to zero, and the nonlinear dynamics is given by $f_D(t, x, a) = (2 - 0.5x_2^2 + a_1, a_2)$, with $A := \{a \in \mathbb{R}^2 \mid \|a\| = (a_1^2 + a_2^2)^{1/2} = 1\}$. The swimmer has unit speed and can move in any direction $a \in A$; the current has speed $2 - 0.5x_2^2$ and flows in the direction $(1, 0)$. The target is the set $\mathcal{X} = \{x \mid v_0(x) \leq 0\}$, where $v_0(x) = C \min(\|(x_1 - 1, x_2)\| - r, r)$ with $r = 0.25$ and $C = 20$. In order to take into account the presence of the two obstacles, we follow the level set approach,

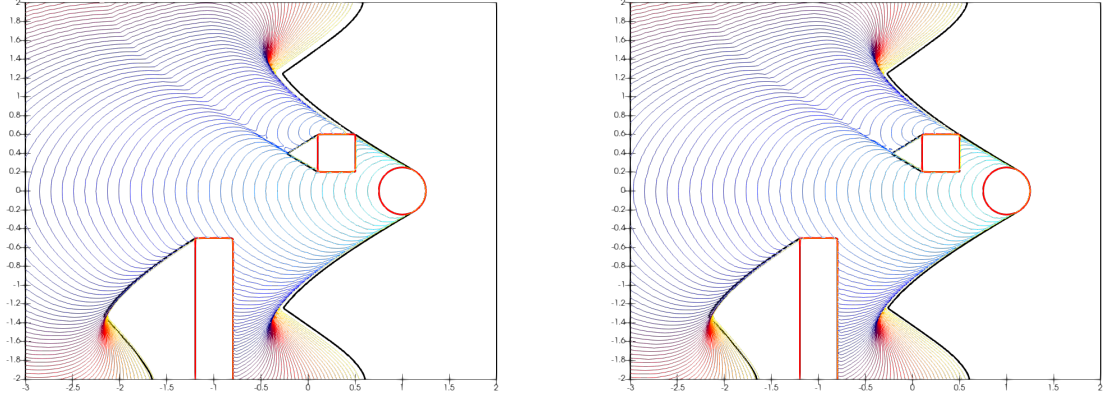


Figure 8: Reachable sets (5.9) computed at each time step for Test 5 on a grid 101×81 and $T = 3$, using WENO (left) and CWENO (right) reconstructions. In both panel the black line represents a reference solution computed on a grid 1001×801 , the red circle represents the target and the red rectangles represent the obstacles.

grid	WENO	CWENO		CWENOZ	
	CPU time	CPU time	% gain	CPU time	% gain
126×126	$6.28e + 00$	$5.34e + 00$	14.94	$5.30e + 00$	15.66
251×251	$4.56e + 01$	$3.96e + 01$	13.04	$3.96e + 01$	13.06
501×501	$3.61e + 02$	$3.11e + 02$	13.87	$3.20e + 02$	11.50
1001×1001	$2.81e + 03$	$2.43e + 03$	13.64	$2.40e + 03$	14.59
2001×2001	$2.20e + 04$	$1.92e + 04$	13.01	$1.89e + 04$	14.00

Table 10: CPU times for Test 5, WENO and CWENO schemes.

as proposed in [BFZ10], and represent the set of constrained states as $\mathcal{K} = \{x \in \mathbb{R}^2 \mid g(x) \leq 0\}$ where

$$g(x) = \max\left(-\gamma, C(\gamma - \max(|x_1 - 0.3|, |x_2 - 0.4|)), C(\gamma - \max(|x_1 + 1|, |x_2 + 1.5|))\right),$$

with $C = 20$, $\gamma = 0.2$.

For every $t \in [0, T]$, the set of points from which the swimmer can reach the target *before time* t (Backward Reachable set) is represented by the level set $\mathcal{R}[0, t] = \{x \in \mathbb{R}^2 \mid \exists s \in [0, t], v(x, s) \leq 0\}$ where v is the solution to a constrained version of (1.1)

$$\min(v_t + H(t, x, Dv), v - g(x)) = 0 \quad (5.8)$$

with initial condition $v(x, 0) = \max(v_0(x), g(x))$, (see [BFZ10, Remark 2]). The space domain is defined as $[-3, 2] \times [-2, 2]$ and the final time to $T = 3$. By using scheme (2.1), we discretize (5.8) as

$$\min(u_i^{n+1} - \min_{\underline{a} \in A^\nu} \{R[u^n](y_i^n(\underline{a}))\}, u_i^{n+1} - g(x_i)) = 0,$$

resulting in the following time marching scheme

$$u_i^{n+1} = \max\left(\min_{\underline{a} \in A^\nu} \{R[u^n](y_i^n(\underline{a}))\}, g(x_i)\right),$$

from which we define the numerical approximation of the seachable set $\mathcal{R}[0, t_n]$ as

$$\mathcal{R}^n = \{x_i \mid \exists k \in \{0, \dots, n\}, u_i^k \leq 0\}. \quad (5.9)$$

The solution is computed with RK3 and $\Delta t = \Delta x$. In Figure 8, we show that, even in this very complex situation, no relevant difference in the accuracy of the computed solution can be observed between the WENO and the Central WENO approaches. On the other hand, Central reconstruction schemes provide a reduction of about 13 – 14% of the computational time.

Conclusion

In this study, a high order semi-Lagrangian scheme has been developed to approximate first order Hamilton–Jacobi–Bellman equations. The primary challenge lies in the nonsmooth nature of the solutions, which would lead to spurious oscillations when using unlimited high order polynomial interpolation.

To address this issue, the reconstruction of the solution at the previous time step at the foot of characteristics has to be performed with a non-oscillatory scheme. Since one has to perform very many interpolations during the minimization procedure, a CWENO technique was proposed to be coupled with the semi-Lagrangian approach. Our study demonstrates that, in terms of errors, our new scheme maintains the favorable behavior of WENO schemes of [CFR06], producing about 30% more accurate results in smooth regions at the price of some extra over/undershoots. However, its computational cost is significantly lower, by a 10 – 30% depending on the specific test.

Additionally, we have established a convergence result in a simpler case, and provided several numerical simulations to further validate the effectiveness of our proposed scheme.

Future Directions

Future research directions could explore the inclusion of high order treatments for boundary conditions and extensions of the convergence analysis to more general Hamiltonians. Investigating the scheme's performance in more complex scenarios would also contribute to a comprehensive understanding of its capabilities.

Acknowledgments

The first two authors would like to thank the Italian Ministry of Instruction, University and Research (MIUR) for supporting this research with funds coming from the PRIN Project 2022 (2022238YY5, entitled "Optimal control problems: analysis, approximation"). All authors are members of the GNCS-INdAM Gruppo Nazionale per il Calcolo Scientifico of Istituto Nazionale di Alta Matematica, Francesco Severi, P.le Aldo Moro, Roma, Italy.

References

- [Abg94] R. Abgrall. On essentially non-oscillatory schemes on unstructured meshes: analysis and implementation. *J. Comput. Phys.*, 114(6):45–48, 1994.
- [BBMZ19] A. Baeza, R. Bürger, P. Mulet, and D. Zorío. Central WENO schemes through a global average weight. *J. Sci. Comput.*, 78(1):499–530, 2019.
- [BCCF21] L. Bonaventura, E. Calzola, E. Carlini, and R. Ferretti. Second order fully semi-Lagrangian discretizations of advection-diffusion-reaction systems. *J. Sci. Comput.*, 88(23), 2021.
- [BCD97] M. Bardi and I. Capuzzo-Dolcetta. *Optimal control and viscosity solutions of Hamilton-Jacobi-Bellman equations*. Systems & Control: Foundations & Applications. Birkhäuser Boston, Inc., Boston, MA, 1997. With appendices by Maurizio Falcone and Pierpaolo Soravia.
- [BFS16] O. Bokanowski, M. Falcone, and S. Sahu. An efficient filtered scheme for some first order time-dependent Hamilton-Jacobi equations. *SIAM J. Sci. Comput.*, 38(1):A171–A195, 2016.
- [BFZ10] O. Bokanowski, N. Forcadel, and H. Zidani. Reachability and minimal times for state constrained nonlinear problems without any controllability assumption. *SIAM J. Control Optim.*, 48(7):4292–4316, 2010.
- [BGFB20] D. S. Balsara, S. Garain, V. Florinski, and W. Boscheri. An efficient class of WENO schemes with adaptive order for unstructured meshes. *J. Comput. Phys.*, 404:109062, 2020.
- [CCDS23] E. Calzola, E. Carlini, X. Dupuis, and F. J. Silva. A semi-Lagrangian scheme for Hamilton-Jacobi-Bellman equations with oblique derivatives boundary conditions. *Numer. Math.*, 153(1):49–84, 2023.
- [CFR06] E. Carlini, R. Ferretti, and G. Russo. A weighted essentially nonoscillatory, large time-step scheme for Hamilton-Jacobi equations. *SIAM J. Sci. Comput.*, 27(3):1071–1091, 2006.

- [CPSV18] I. Cravero, G. Puppo, M. Semplice, and G. Visconti. CWENO: uniformly accurate reconstructions for balance laws. *Math. Comp.*, 87(312):1689–1719, 2018.
- [CS19] M. J. Castro and M. Semplice. Third- and fourth-order well-balanced schemes for the shallow water equations based on the CWENO reconstruction. *Int. J. Numer. Meth. Fluid.*, 89(8):304–325, 2019.
- [CSV19] I. Cravero, M. Semplice, and G. Visconti. Optimal definition of the nonlinear weights in multidimensional Central WENOZ reconstructions. *SIAM J. Numer. Anal.*, 57(5):2328–2358, 2019.
- [DBSR17] M. Dumbser, W. Boscheri, M. Semplice, and G. Russo. Central weighted ENO schemes for hyperbolic conservation laws on fixed and moving unstructured meshes. *SIAM J. Sci. Comput.*, 39(6):A2564–A2591, 2017.
- [Fer02] R. Ferretti. Convergence of semi-Lagrangian approximations to convex Hamilton-Jacobi equations under (very) large Courant numbers. *SIAM J. Numer. Anal.*, 40(6):2240–2253, 2002.
- [FF94] M. Falcone. and R. Ferretti. Discrete time high-order schemes for viscosity solutions of Hamilton-Jacobi-Bellman equations. *Numer. Math.*, 67(3):315–344, 1994.
- [FF02] M. Falcone. and R. Ferretti. Semi-Lagrangian schemes for Hamilton-Jacobi equations, discrete representation formulae and Godunov methods. *J. Comput. Phys.*, 175(2):559–575, 2002.
- [FF14] M. Falcone. and R. Ferretti. *Semi-Lagrangian approximation schemes for linear and Hamilton-Jacobi equations*. Society for Industrial and Applied Mathematics (SIAM), Philadelphia, PA, 2014.
- [FPT20a] M. Falcone, G. Paolucci, and S. Tozza. Convergence of adaptive filtered schemes for first order evolutionary Hamilton-Jacobi equations. *Numer. Math.*, 145(2):271–311, 2020.
- [FPT20b] M. Falcone, G. Paolucci, and S. Tozza. Multidimensional smoothness indicators for first-order Hamilton-Jacobi equations. *J. Comput. Phys.*, 409, 2020.
- [HEOC87] A. Harten, B. Engquist, S. Osher, and S. R. Chakravarthy. Uniformly high-order accurate essentially nonoscillatory schemes III. *J. Comput. Phys.*, 71(2):231–303, 1987.
- [HS99] C. Hu and C. W. Shu. Weighted essentially non-oscillatory schemes on triangular meshes. *J. Comput. Phys.*, 150(1):97–127, 1999.
- [HT03] T. Y. Hou and E. Tadmor, editors. *High-Order Schemes for Multi-Dimensional Hamilton-Jacobi Equations*, Berlin, Heidelberg, 2003. Springer Berlin Heidelberg.
- [JP00] G.-S. Jiang and D. Peng. Weighted ENO schemes for Hamilton-Jacobi equations. *SIAM J. Sci. Comput.*, 21(6):2126–2143, 2000.
- [JS96] G. S. Jiang and C. W. Shu. Efficient implementation of weighted ENO schemes. *J. Comput. Phys.*, 126:202–228, 1996.

- [LOC94] X. D. Liu, S. Osher, and T. Chan. Weighted essentially non-oscillatory schemes. *J. Comput. Phys.*, 115(1):200–212, 1994.
- [LPR00] D. Levy, G. Puppo, and G. Russo. Compact central WENO schemes for multidimensional conservation laws. *SIAM J. Sci. Comput.*, 22(2):656–672, 2000.
- [LT00] C. T. Lin and E. Tadmor. High-resolution nonoscillatory central schemes for Hamilton-Jacobi equations. *SIAM J. Sci. Comput.*, 21(6):2163–2186, 2000.
- [OS91] S. Osher and C. W. Shu. High-order essentially non-oscillatory schemes for Hamilton-Jacobi equation. *SIAM J. Numer. Anal.*, 28:907–922, 1991.
- [SCR16] M. Semplice, A. Coco, and G. Russo. Adaptive mesh refinement for hyperbolic systems based on third-order Compact WENO reconstruction. *J. Sci. Comput.*, 66:692–724, 2016.
- [SV20] M. Semplice and G. Visconti. Efficient implementation of adaptive order reconstructions. *J. Sci. Comput.*, 83(1), 2020.
- [ZCZ08] J. Zhou, L. Cai, and F.-Q. Zhou. New high-resolution scheme for three-dimensional nonlinear hyperbolic conservation laws. *Appl. Math. Comp.*, 198(2):770–786, 2008.
- [Zen86] M. Zennaro. Natural continuous extensions of Runge-Kutta methods. *Math. Comp.*, 46(173):119–133, 1986.
- [ZQ16] J. Zhu and J. Qiu. A new fifth order finite difference WENO scheme for solving hyperbolic conservation laws. *J. Comput. Phys.*, 318:110–121, 2016.
- [ZQ17] J. Zhu and J. Qiu. A new fifth order finite difference WENO scheme for Hamilton-Jacobi equations. *Numer. Meth. for PDEs*, 33(4):1095–1113, 2017.
- [ZQ20] J. Zhu and J. Qiu. A new type of high-order WENO schemes for Hamilton-Jacobi equations on triangular meshes. *Comm. Computat. Phys.*, 27(3):897–920, 2020.
- [ZSQ19] F. Zheng, C. W. Shu, and J. Qiu. High order finite difference Hermite WENO schemes for the Hamilton–Jacobi equations on unstructured meshes. *Comp. & Fluids*, 183:53–65, 2019.

Appendix

We report here the matrix involved in the definition (3.16).

$$A_{\text{sw}} = \begin{pmatrix} \frac{857}{720} & \frac{-109}{45} & \frac{827}{720} & 0 & \frac{-109}{45} & \frac{887}{180} & \frac{-421}{180} & 0 & \frac{827}{720} & \frac{-421}{180} & \frac{827}{720} & \frac{-421}{180} & \frac{797}{720} & 0 & 0 & 0 & 0 & 0 & 0 \\ \frac{-109}{45} & \frac{571}{90} & \frac{-293}{90} & 0 & \frac{887}{180} & \frac{-1157}{90} & \frac{1187}{180} & 0 & \frac{-293}{90} & \frac{1187}{180} & \frac{-421}{180} & \frac{278}{45} & \frac{-571}{180} & 0 & 0 & 0 & 0 & 0 & 0 \\ \frac{827}{720} & \frac{-293}{90} & \frac{1817}{720} & 0 & \frac{-421}{180} & \frac{1187}{180} & \frac{-229}{45} & 0 & \frac{797}{720} & \frac{-571}{180} & \frac{797}{720} & \frac{-571}{180} & \frac{1787}{720} & 0 & 0 & 0 & 0 & 0 & 0 \\ 0 & 0 & 0 & 0 & 0 & 0 & 0 & 0 & 0 & 0 & 0 & 0 & 0 & 0 & 0 & 0 & 0 & 0 & 0 \\ \frac{-109}{45} & \frac{887}{180} & \frac{-421}{180} & 0 & \frac{571}{90} & \frac{-1157}{90} & \frac{278}{45} & 0 & \frac{-293}{90} & \frac{1187}{180} & \frac{-421}{180} & \frac{1187}{180} & \frac{-571}{180} & 0 & 0 & 0 & 0 & 0 & 0 \\ \frac{887}{180} & \frac{-1157}{90} & \frac{1187}{180} & 0 & \frac{-1157}{90} & \frac{1472}{45} & \frac{-1547}{90} & 0 & \frac{1187}{180} & \frac{-1547}{90} & \frac{1187}{180} & \frac{-1547}{90} & \frac{1667}{180} & 0 & 0 & 0 & 0 & 0 & 0 \\ \frac{-421}{180} & \frac{1187}{180} & \frac{-229}{45} & 0 & \frac{278}{45} & \frac{-1547}{90} & \frac{1141}{90} & 0 & \frac{-571}{180} & \frac{1667}{180} & \frac{-571}{180} & \frac{1667}{180} & \frac{-623}{90} & 0 & 0 & 0 & 0 & 0 & 0 \\ 0 & 0 & 0 & 0 & 0 & 0 & 0 & 0 & 0 & 0 & 0 & 0 & 0 & 0 & 0 & 0 & 0 & 0 & 0 \\ \frac{827}{720} & \frac{-421}{180} & \frac{797}{720} & 0 & \frac{-293}{90} & \frac{1187}{180} & \frac{-571}{180} & 0 & \frac{1817}{720} & \frac{-229}{45} & \frac{1817}{720} & \frac{-229}{45} & \frac{1787}{720} & 0 & 0 & 0 & 0 & 0 & 0 \\ \frac{-421}{180} & \frac{278}{45} & \frac{-571}{180} & 0 & \frac{1187}{180} & \frac{-1547}{90} & \frac{1141}{90} & 0 & \frac{-229}{45} & \frac{1141}{90} & \frac{-229}{45} & \frac{1141}{90} & \frac{-623}{90} & 0 & 0 & 0 & 0 & 0 & 0 \\ \frac{797}{720} & \frac{-571}{180} & \frac{1787}{720} & 0 & \frac{1787}{720} & \frac{1667}{180} & \frac{-623}{90} & 0 & \frac{1787}{720} & \frac{-623}{90} & \frac{1787}{720} & \frac{-623}{90} & \frac{3497}{720} & 0 & 0 & 0 & 0 & 0 & 0 \\ 0 & 0 & 0 & 0 & 0 & 0 & 0 & 0 & 0 & 0 & 0 & 0 & 0 & 0 & 0 & 0 & 0 & 0 & 0 \\ 0 & 0 & 0 & 0 & 0 & 0 & 0 & 0 & 0 & 0 & 0 & 0 & 0 & 0 & 0 & 0 & 0 & 0 & 0 \\ 0 & 0 & 0 & 0 & 0 & 0 & 0 & 0 & 0 & 0 & 0 & 0 & 0 & 0 & 0 & 0 & 0 & 0 & 0 \\ 0 & 0 & 0 & 0 & 0 & 0 & 0 & 0 & 0 & 0 & 0 & 0 & 0 & 0 & 0 & 0 & 0 & 0 & 0 \end{pmatrix}$$

$$A_{\text{opt}}^{(2)} = \begin{pmatrix} 10859 & -58881 & 221047 & -363499 & -13889 & 871553 & -363499 & 66427 \\ 2700 & 5600 & 25200 & 151200 & 12600 & 302400 & 151200 & 100800 \\ -58881 & 426623 & -1536757 & 221047 & 871553 & -11137 & 841823 & -363499 \\ 5600 & 12600 & 50400 & 25200 & 302400 & 1200 & 100800 & 151200 \\ 221047 & -1536757 & 426623 & -58881 & -363499 & 841823 & -11137 & 871553 \\ 25200 & 50400 & 12600 & 151200 & 100800 & 100800 & 1200 & 302400 \\ -363499 & 221047 & -58881 & 66427 & 66427 & -363499 & 871553 & -13889 \\ 151200 & 25200 & 5600 & 100800 & 100800 & 151200 & 302400 & 12600 \\ -58687 & 1226693 & -1536757 & 841823 & 10859 & -58881 & 221047 & -363499 \\ 4200 & 33600 & 100800 & 100800 & 2700 & 5600 & 25200 & 151200 \\ 1226693 & -2958593 & 10709107 & -1536757 & -58881 & 426623 & -1536757 & 221047 \\ 33600 & 25200 & 100800 & 50400 & 5600 & 12600 & 50400 & 25200 \\ -1536757 & 10709107 & -100800 & -2958593 & 221047 & -1536757 & 426623 & -58881 \\ 50400 & 100800 & 100800 & 25200 & 25200 & 50400 & 12600 & 5600 \\ 841823 & -1536757 & 1226693 & -58687 & -363499 & 221047 & -58881 & 10859 \\ 100800 & 50400 & 33600 & 4200 & 151200 & 25200 & 5600 & 2700 \\ 48799 & -340087 & 426623 & -11137 & -182131 & 60463 & -58881 & 871553 \\ 3150 & 8400 & 12600 & 1200 & 37800 & 4800 & 5600 & 302400 \\ -340087 & 815527 & -2958593 & 426623 & 60463 & -340087 & 1226693 & -58881 \\ 8400 & 6300 & 25200 & 12600 & 4800 & 8400 & 33600 & 5600 \\ 426623 & -2958593 & 815527 & -340087 & -58881 & 1226693 & -340087 & 60463 \\ 12600 & 25200 & 6300 & 8400 & 5600 & 33600 & 8400 & 4800 \\ -11137 & 426623 & -340087 & 48799 & 871553 & 60463 & 60463 & -182131 \\ 1200 & 12600 & 8400 & 3150 & 302400 & -58881 & 4800 & 37800 \\ -182131 & 60463 & -58881 & 871553 & 2903 & -182131 & 10859 & -13889 \\ 37800 & 4800 & 5600 & 302400 & 1575 & 37800 & 2700 & 12600 \\ 60463 & -340087 & 1226693 & -58881 & -182131 & 48799 & -58687 & 10859 \\ 4800 & 8400 & 33600 & 5600 & 37800 & 3150 & 4200 & 2700 \\ -58881 & 1226693 & -340087 & 60463 & 10859 & -58687 & 48799 & -182131 \\ 5600 & 33600 & 8400 & 4800 & 2700 & 4200 & 3150 & 37800 \\ 871553 & -58881 & 60463 & -182131 & -13889 & -182131 & -182131 & 2903 \\ 302400 & 5600 & 4800 & 37800 & 12600 & 37800 & 37800 & 1575 \end{pmatrix}$$